Relationship between Excitation Energy Transfer, Trapping, and Antenna Size in Photosystem II†

Laura M. C. Barter,‡,§ Maria Bianchietti,‡ Chris Jeans,§ Maria J. Schilstra,§ Ben Hankamer,‡ Bruce A. Diner,|| James Barber,‡ James R. Durrant,§ and David R. Klug*,§

Departments of Biochemistry and Chemistry, Imperial College, London SW7 2AY, U.K., and Experimental Station, E. I. Du Pont de Nemours & Company, Wilmington, Delaware 19880-0173

Received July 25, 2000; Revised Manuscript Received January 9, 2001

ABSTRACT: We present a systematic study of the effect of antenna size on energy transfer and trapping in photosystem II. Time-resolved fluorescence experiments have been used to probe a range of particles isolated from both higher plants and the cyanobacterium *Synechocystis* 6803. The isolated reaction center dynamics are represented by a quasi-phenomenological model that fits the extensive time-resolved data from photosystem II reaction centers and reaction center mutants. This representation of the photosystem II "trapping engine" is found to correctly predict the extent of, and time scale for, charge separation in a range of photosystem II particles of varying antenna size (8−250 chlorins). This work shows that the presence of the shallow trap and slow charge separation kinetics, observed in isolated D1/D2/cyt *b*559 reaction centers, are indeed retained in larger particles and that these properties are reflected in the trapping dynamics of all larger photosystem II preparations. A shallow equilibrium between the antennae and reaction center in photosystem II will certainly facilitate regulation via nonphotochemical quenching, and one possible interpretation of these findings is therefore that photosystem II is optimized for regulation rather than for efficiency.

The light-driven reactions that take place in photosystem II culminate with the splitting of water to release oxygen (for a review see ref *1*). Photosystem II contains the redox-active reaction center comprising the D1 and D2 proteins and the α and *β* subunits of the cytochrome *b*559. These proteins support six chlorophyll *a* molecules, two pheophytin *a* molecules, two *β* carotenes, and one cytochrome *b*559 (*2*, *3*). In higher plants, approximately 250 molecules of chlorophyll surround the reaction center; they function as antenna by absorbing photons and allowing their transfer to the reaction center. The reaction center itself comprises a weakly coupled multimer of four chlorophyll and two pheophytin molecules (*4*). Following the excitation of these pigments by light, a charge separation reaction takes place, leading to the formation of the primary radical pair P_{680}^+ $Pheo^-$ (*5*). Secondary charge transfer reactions then occur to the plastoquinones (Q_A and Q_B), resulting in P_{680}^+ Q_A^- and subsequently P_{680}^+ Q_B^- formation (*1*). Figure 1 qualitatively summarizes pictorially the energy equilibration and primary electron transfer processes that take place in the photosystem II reaction center. This picture has been constructed from a number of our studies made over the past decade (*4*, *6*−*11*).

Photosystem II is surprisingly sensitive to photoinduced damage (*12*) and has adopted a number of regulatory mechanisms in response to environmental stresses (for a review see ref *13*). Under certain conditions quenching centers in the antenna are formed. These protect the reaction center by dissipating excess excitation energy in a process known as nonphotochemical quenching. This process must compete with energy transfer and trapping by the reaction center in order to be effective. A predictive model of energy transfer and trapping in photosystem II is therefore fundamental to the understanding of the balance between the dissipation and utilization of energy in photosystem II. The work that we present here reflects energy transfer and trapping in systems where the regulatory mechanisms are not switched on.

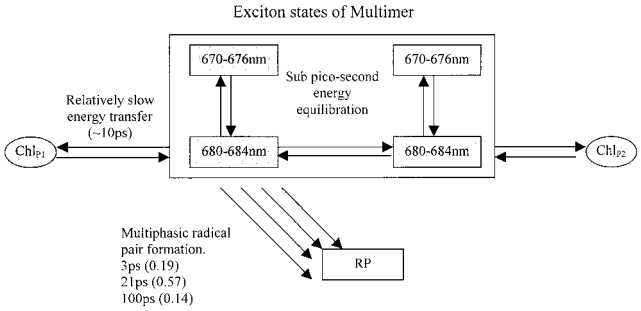

FIGURE 1: Summary of the energy equilibration and primary electron transfer processes in the isolated photosystem II reaction center. Subpicosecond energy transfer within the P_{680} multimer and slower energy transfer from the peripheral chlorophylls (Chl_{P1} and Chl_{P2}) are included. Both of the 670−676 nm states shown are assumed to be 2-fold degenerate. An indication of the multiexponential nature of radical pair formation is also given, with values of the lifetimes (and amplitudes in parentheses) as found in refs *8*, *9*, and *17*.

† This work was financially supported by the BBSRC.

* Corresponding author. Fax: 44171-594-5806. E-mail: d.klug@ic.ac.uk.

‡ Department of Biochemistry, Imperial College.

§ Department of Chemistry, Imperial College.

|| E. I. Du Pont de Nemours & Co.

10.1021/bi001724q CCC: $20.00
Published on Web 03/09/2001

One way to study energy transfer and trapping is to break down the photosystem II complex into smaller components. The smallest charge separating unit that can be isolated from photosystem II *(14, 15)* is the D1/D2/cytochrome *b*559 reaction center itself, which loses its secondary electron acceptors (quinones) during the isolation procedure. Moreover, as the isolated reaction center does not contain antenna complexes, the radical pairs formed by charge separation are more easily identified by transient absorption spectroscopy, as are the roles of the individual pigments/states. Work on the isolated reaction center has enabled an understanding to be gained of the subpicosecond equilibration of the excitation energy within the majority of the reaction center chlorins (*6, 11*) as well as the slow energy transfer from the peripheral chlorophylls (*10, 16*). The primary charge separation reactions have also been extensively studied and have been found to exhibit multiexponential kinetics with lifetimes (and amplitudes) of 3 ps (0.19), 21 ps (0.57), 100 ps (0.14), and >100 ps (0.10) *(8, 9, 17)*. [Similar data were obtained by other groups *(18*−*21)*.]

Studies on isolated photosystem II reaction centers have also highlighted significant mechanistic differences between the photosynthetic reaction centers from purple bacteria and photosystem II. The radical pair free energy in both systems is time dependent; however, at any given time the free energy gap in the bacterial system is found to be larger than in photosystem II. For example, the photosystem II reaction center has a primary radical pair P_{680}^+ $Pheo^-$ which is ∼100 meV below the singlet states (on nanosecond time scales at 277 K) (*22, 23*), whereas *Rhodobacter sphaeroides* has a free energy gap of ∼250 meV in quinone depleted and reduced reaction centers at these times (*24*−*26*). The small energy gaps that drive the photochemistry in photosystem II reaction centers lead to the formation of shallow equilibrium between the radical pair states and singlet states (*27*). This causes the reaction center kinetics to be highly sensitive to genetically modified changes in the redox potential of the chlorin anions and cations (*28*). A microscopic model describing energy transfer in the reaction center has been shown to be consistent with the measured energy transfer dynamics (*29, 30, 31*).

In this paper we employ a phenomenological model describing energy transfer and trapping in the photosystem II reaction center to explain the antenna size dependence of this process in photosystem II. Although this model can correctly fit both the transient absorption and single photon counting data from isolated photosystem II reaction center samples and reaction center mutants, it should not be mistaken for a microscopic representation of the reaction center dynamics, which will be discussed in more detail elsewhere. In this paper we present a study of energy transfer and trapping as a function of antenna size. A number of photosystem II preparations were examined. These range from isolated D1/D2/*b*559 reaction centers containing 8 chlorins to photosystem II membrane fragments with ∼250 chlorophyll molecules per reaction center. Superficially, it is not obvious that one can reconcile the slow trapping of excitation energy observed in photosystem II reaction centers with that reported in more intact membrane particles such as BBY's. We show, however, that the phenomenological model that correctly fits the reaction center data quantitatively predicts the trapping behavior in photosystem II as a function of antenna size in the absence of secondary electron transfer.

MATERIALS AND METHODS

Sample Preparation. Reaction centers were prepared from pea (*Pisum sativum*) chloroplasts as previously described (*32*) and stored at 77 K. Their pigment stoichiometry was 6 chlorophyll *a* molecules:2 pheophytin *a* molecules:2 β-carotene:1 cytochrome *b*559 (*2, 3*). For optical spectroscopy the samples were resuspended in a buffer containing 20 mM Bis-Tris, 20 mM NaCl, 10 mM $MgCl_2 \cdot 6H_2O$, and 1.5 mM *n*-dodecyl β-D-maltoside at pH 6.5.

Monomeric and dimeric CP47 reaction center complexes were obtained from BBY-type PS II membrane fragments isolated from spinach with modifications described by Hankamer and co-workers (*33*). After being washed with 50 mM Tris-HCl, the BBYs were solubilized, and the monomer and dimer CP47 complexes were isolated and characterized as described (*34, 35*). It should be noted that the monomeric complexes do not bind functional Q_A. For the experiments described in this paper, the samples were resuspended in a buffer containing 20 mM Bis-Tris, 20 mM NaCl, 10 mM $MgCl_2 \cdot 6H_2O$, and 1.5 mM *n*-dodecyl β-D-maltoside at pH 6.5.

Dimeric CP43 CP47 reaction center complexes were isolated from oxygen-evolving photosystem II cores (OctGlc cores) as described (*36*) and were stored at 77 K. In the optical experiments described here, the samples were diluted in a buffer containing 0.3 M sucrose, 25 mM MES, 10 mM $MgCl_2$, 10 mM NaCl, 5 mM $CaCl_2$, and 1.5 mM *n*-dodecyl β-D-maltoside at pH 6.5.

The PS II−LHC II supercore complexes were prepared by solubilization of BBY-type PS II membrane fragments with 20 mM dodecyl maltoside and sucrose gradient centrifugation as described previously (*37*). The sucrose gradient contained 1 M glycine−betaine as described in Boekema et al. (*37*). The samples were stored at 77 K. For experimentation the samples were resuspended in 0.3 M sucrose, 25 mM MES, 10 mM $MgCl_2$, 10 mM NaCl, 5 mM $CaCl_2$, and 0.03% w/v *n*-dodecyl β-D-maltoside at pH 6.5.

The oxygen evolving PS II membrane fragments (BBYs) (*38*), were prepared as described previously (*39*). For the spectroscopy presented here the samples were resuspended in 0.3M Sucrose 25 mM MES, 10 mM $MgCl_2$, 10 mM NaCl, and 5 mM $CaCl_2$ at pH 6.5.

Manganese-depleted CP43 CP47 photosystem II core complexes from *Synechocystis* 6803 mutant and wild type were prepared as described in Tang et al. (*40*). Samples were desalted and suspended in 50 mM MES−NaOH, pH 6.0, containing 20 mM $CaCl_2$, 5 mM $MgCl_2$, 25% (w/v) glycerol, and 0.03% dodecyl maltoside. Final concentrations were typically 5−10 mg of Chl/mL and were stored at −80 °C. For the experiments described in this paper, samples were resuspended in a buffer containing 0.3 M sucrose 25 mM MES, 10 mM $MgCl_2$, 10 mM NaCl, 5 mM $CaCl_2$, and 1.5 mM *n*-dodecyl β-D-maltoside at pH 6.5.

Sample preparation was carried out immediately prior to the optical experiments. Samples were diluted, using the buffers described above, into a 1 cm^3 reduced volume fluorescence cuvette to give a final concentration of ∼3 μg mL^{-1}. Anaerobic conditions were achieved by the addition

of 5 mM glucose, 0.1 mg mL^{-1} glucose oxidase, and 0.05 mg mL^{-1} catalase. The position of the chlorophyll Q_y band absorption maximum was used as a monitor of the stability of the sample. It was ensured that this peak shifted by less than 1 nm during the course of an experiment. This is indicative of less than 10% activity loss in isolated reaction center samples (*41*).

Time-Resolved Single Photon Counting. The time-resolved single photon counting apparatus has been described in full detail in ref *22*. A mode-locked coherent YAG laser synchronously pumps a DCM dye laser. The cavity dumped output has a repetition rate of 5 MHz and an 8 ps pulse duration.

The data presented from the isolated D1/D2/cyt *b*559 reaction centers, monomeric and dimeric CP47/D1/D2/cyt *b*559 complexes, and the BBY PS II membrane fragments were collected with an instrument response measured to have a fwhm of 36 ps using a LUDOX scattering solution. The experiments carried out on the dimeric CP43/CP47/D1/D2/cyt *b*559 cores, supercore complexes, and the *Synechocystis* 6803 wild-type and D1-His198Ala monomeric CP43 CP47 reaction center complexes used an instrument response fwhm of 90 ps. The effect of the different instrument response functions was tested on isolated D1/D2/cyt *b*559 samples. Differences in the multiexponential fits to the data were only apparent at times earlier than 100 ps. As the work that we present monitors the singlet state population at 150 and 250 ps, the different instrument response functions will not affect the results that we discuss.

All of the samples were excited using an excitation wavelength of 620 nm, and all of the emission was collected to the red of a 640 nm high-pass filter. The incident light intensity used for each experiment varied but was chosen to ensure that each sample was fully closed, i.e., Q_A prereduced (see Results section). The laser beam spot diameter used during the experiments was ~4 mm. Throughout the experiments the samples were chilled to 4 °C and stirred continuously. The fluorescence decay kinetics did not alter during the 15 min data acquisition time.

The data were analyzed assuming multiexponential kinetics to allow deconvolution of the instrument response function and as a method of representing the data mathematically.

Measurement of Absolute Singlet State Populations. Rather than focusing on a lifetime analysis, all of the data presented allows the singlet state populations to be tracked during the trapping process. A comparison of the singlet state populations from samples relies on the precise scaling of each data set by the number of photons absorbed and the photon detection geometry. The optical densities of each sample were therefore recorded, and changes in laser power and photon number reaching the detection system were also monitored using dye standards.

An absolute scale for the singlet state populations in all the samples was found by using the isolated reaction center data as a standard. The equilibrium constants and hence the singlet state populations from the reaction center have already been established using combined results from transient absorption and time-resolved fluorescence experiments via a comparison with chlorophyll *a* (*22*). The use of the reaction center standard enabled the decays from all of the different preparations to be compared on an absolute scale.

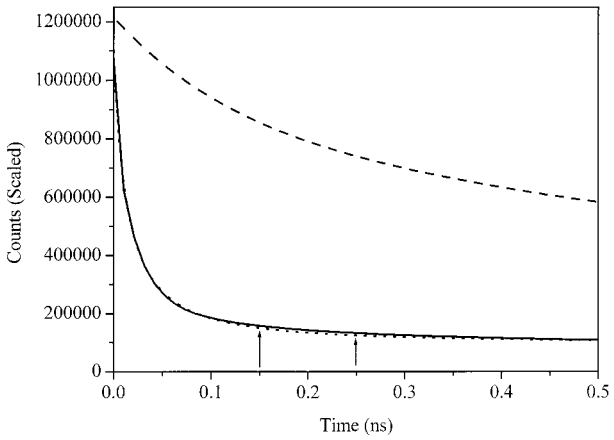

FIGURE 2: Excited-state decay kinetics for isolated photosystem II reaction centers (—) and BBY's (- - -). The isolated reaction center kinetics were obtained using a combined analysis of transient absorption, fluorescence up conversion, and time-resolved single photon counting data, allowing resolution of the fast components. The BBY fit was obtained from the single photon counting data alone. This is making a comparison between absolute singlet state populations of both of the samples. Also shown (···) are the isolated reaction center excited singlet state decay kinetics calculated from a three-state model with inhomogeneously broadened energies of the radical pair states (see text for details).

Test of the Accuracy of the Scaling Method. Figure 2 is shown to give the reader a feel for the accuracy of the use of the dye and reaction center standards as a method of referring the data to an absolute population scale. Fits to the experimental data obtained from isolated reaction center samples and PS II membrane fragments (BBY's) are compared in Figure 2. The fit to the reaction center has been obtained by the combined use of transient absorption and single photon counting data, which allows the fast components (that could not be resolved using single photon counting alone) to be included in the fit. The fits to the singlet state decay kinetics, obtained using single photon counting, from the largest particle, namely the BBY's (shown in Figure 2), are the results that should have the smallest contribution from fast components. We find that there is only a 9% discrepancy in the value of the singlet state population at $t = 0$ between the exponential fits to the reaction center and the BBY data, which gives confidence in the method used to scale the data presented here. It should be emphasized that measurement of the singlet state populations at $t = 0$ ps has not been used as the method of scaling the data. The data at early times has only been included here to indicate the accuracy of the scaling. The value of 9% should not be taken as a definitive level of the accuracy of these experiments, as it includes the imprecision caused by the finite length of the instrument response function. Both the precision and accuracy of the data at $t = 150$ and 250 ps (indicated by the arrows on Figure 2) should be considerably better than that at $t = 0$ ps.

One way of representing the data obtained from all of the preparations is to compare the absolute singlet state populations at a particular time. To make a comparison between the various samples, the effective antenna size of each sample must be calculated. For such calculations, a weighting of chlorophyll *b* (present in some of the samples) to chlorophyll *a* was taken as 1:6 in order to account for the free energy difference between the energies of their respective excited states (see Table 1).

Table 1: Summary of the Composition of the Samples Studied

sample	no. of Chl *a* molecules in the antenna (per reaction center)	no. of Chl *b* molecules in the antenna (per reaction center)	total no. of chlorins in each sample	total no. of effective chlorins in each sample[a]
D1/D2/*b*559 reaction center			8	8
monomeric CP47 D1/D2/*b*559 reaction center	10 ± 1.1		18 ± 1.1	18
dimeric CP47 D1/D2/*b*559 reaction center	14 ± 2.3		22 ± 2.3	22
dimeric CP43 CP47 D1/D2/b559 reaction center core	32.5 ± 2.1	1.09 ± 0.03	41.59 ± 2.13	41
LHC II supercore complex	72.0 ± 8.8	23 ± 3.6	103.0 ± 12.4	84
BBY photosystem II membrane fragments	158 ± 3	86 ± 3	252 ± 6	179
wild-type *Synechocystis* 6803 monomeric CP43 CP47 D1/D2/*b*559 reaction center complexes	32 ± 2		40 ± 2	40
His198Ala *Synechocystis* 6803 monomeric CP43 CP47 D1/D2/*b*559 reaction center complexes	32 ± 2		40 ± 2	40

[a] The effective number of chlorins has been calculated as described in Materials and Methods.

$$\mathbf{RC^* \underset{k_{-1}}{\overset{k_{+1}}{\Leftrightarrow}} RP1 \underset{k_{-2}}{\overset{k_{+2}}{\Leftrightarrow}} RP2} \quad \text{(a)}$$

$$\mathbf{Ant^* \underset{k_{-}}{\overset{k_{+}}{\Leftrightarrow}} RC^* \underset{k_{-1}}{\overset{k_{+1}}{\Leftrightarrow}} RP1 \underset{k_{-2}}{\overset{k_{+2}}{\Leftrightarrow}} RP2} \quad \text{(b)}$$

$$\mathbf{(Ant\ RC)^* \underset{k_{-1}}{\overset{k_{+1}}{\Leftrightarrow}} RP1 \underset{k_{-2}}{\overset{k_{+2}}{\Leftrightarrow}} RP2} \quad \text{(c)}$$

FIGURE 3: (a) Kinetic model describing electron transfer in the reaction center. RC* represents the reaction center excited singlet states; RP1 and RP2 are the radical pair states. k_{+1} and k_{+2} are the forward rate constants, and k_{-1} and k_{-2} are the reverse rate constants. (b) shows the model adapted to take account of the presence of antenna. (c) is mathematically equivalent to (b) when $k_+ + k_- \gg k_{+1} + k_{-1}$.

Reaction Center Kinetic Model, a "Trapping Engine" for Photosystem II. The multiphasic nature of the radical pair formation in the photosystem II reaction center can be modeled in a number of ways. Although a fully microscopic model is required to understand the architecture of the photosystem II reaction center itself, understanding the interaction between antenna size and the reaction center trapping engine only requires the trapping engine to be described by a phenomenological model.

Two-state schemes, with an excited singlet state and one radical pair state, have been discussed previously (*42*, *43*). These models fail to reproduce the antenna size dependence. A reaction scheme that consists of at least three states [excited singlet state RC* and radical pair states RP1 and RP2 (see Figure 3a)] with homogeneous broadening and which represents electron transfer down the active branch of the reaction center is required. RP1 represents the state $Chl_{(1)}^+ Chl_{(2)}^-$, and RP2 represents the radical pair state $Chl_{(1)}^+ Pheo_{(1)}^-$ (see Figure 4). The presence of chlorophyll anions in photosystem II has been demonstrated in experiments on site-directed mutants from *Synechocystis* PCC 6803 reaction centers (*44*) and is believed to play a role in the native higher plant system. The presence of fast intermediate states in charge separation was postulated by Groot et al. (*21*), but as the intermediates are not directly detectable in wild-type reaction centers, no supporting evidence was provided.

Any three-state reaction scheme alone would not be sufficient to account for the wide range of trapping times in the reaction center data. Static energy level disorder is required to recreate the multiexponential kinetics observed for primary charge separation in purple bacterial reaction centers (*45*, *46*) and also in photosystem II (*41*, *47*). It has been shown previously that a two-state model (excited singlet state and one radical pair state) which includes static disorder of the radical pair state energy could not reproduce transient absorption data from isolated photosystem II reaction centers (*48*). We find that a three-state model including inhomogeneously broadened free energies of the radical pair states and representing electron transfer in the active arm of photosystem II (Figure 5) is able to reproduce the experimental results from the isolated reaction center and *Synechocystis* PCC 6803 reaction center mutants. This model

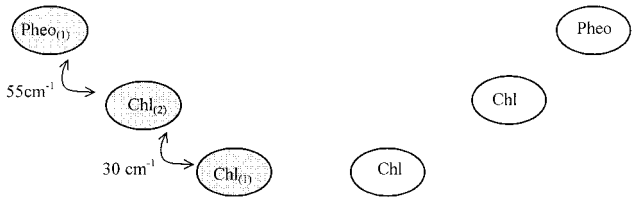

FIGURE 4: The three-state model assumes electron transfer down one arm of the reaction center. RP1 represents $Chl_{(1)}^+ Chl_{(2)}^-$, and RP2 represents $Chl_{(1)}^+ Pheo_{(1)}^-$. The electronic couplings calculated assuming the same distances between chlorins as found in the *Rp. viridis* structure are also shown.

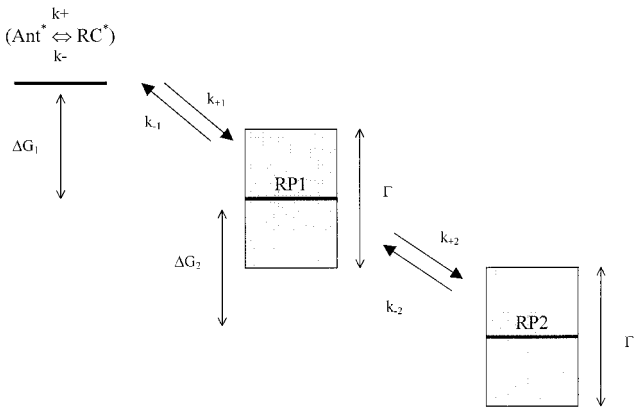

FIGURE 5: Illustration of the three-state phenomenological model with inhomogeneously broadened radical pair state energies. Ant* and RC* represent the excited states of the antenna and the reaction center, respectively, and RP1 and RP2 are radical pair states as described in Figure 4. ΔG_1 is the free energy between the excited singlet states and RP1, and ΔG_2 is the free energy between RP1 and RP2.

is not meant to suggest any literal physical meaning; rather it is simply being used as one way of representing the trapping dynamics in the reaction center. It effectively represents a trapping engine, which causes the free energy of the system to drop over time. For example, the charge separation could actually occur in the reverse order to the labeling of Figure 3.

Conventional nonadiabatic electron transfer theory was employed as a way of including the effect of the inhomogeneous broadening of the radical pair states. The dependence of the rate of electron transfer [k_{+1}, k_{-1}, k_{+2}, k_{-2} (see Figure 5)] upon the free energy gap between the reactant and product (ΔG_1 or ΔG_2) is given by eq 1 (*49*)

$$k_{et} = \frac{2\pi}{\hbar} V^2 \left(\frac{1}{4\pi\lambda kt}\right)^{1/2} \left(\exp\left(-\frac{(-\Delta G - \lambda)^2}{4\lambda kT}\right)\right) \quad (1)$$

where k_{et} is the rate of electron transfer, λ is the reorganization energy, and V is the electronic coupling between the two states. ΔG is the free energy gap between the states [either RC* and RP1 (ΔG_1) or RP1 and RP2 (ΔG_2)].

The static energy level disorder is included in the numerical simulations by ensemble averaging the electron transfer calculations over 1000 reaction centers. For each reaction center calculation the value of the free energy gap ΔG was selected at random from a Gaussian distribution with a mean $\langle \Delta G \rangle$ and width $\Gamma = 850$ cm^{-1} (fwhm). Experimental work by others (*45*, *47*) has indicated similar values of Γ. Parameters used in the calculations were $\langle DG_1 \rangle = 100$ cm^{-1}, $\langle DG_2 \rangle = -1300$ cm^{-1}, and $\lambda = 700$ cm^{-1}. It should be emphasized that the state energies are effectively fitting parameters for the reaction center data but are kept constant in all antenna size modeling. The electronic couplings were calculated assuming the same distances between chlorins as are found in the structure of *Rhodopseudomonas viridis*. The coupling between $Chl_{(1)}$ and $Chl_{(2)}$ (v_1) = 30 cm^{-1} and between $Chl_{(2)}$ and $Pheo_{(1)}$ (v_2) = 55 cm^{-1} (see Figure 4).

The fit to the experimental data and the results for such modeled calculations for the isolated reaction center are overlaid in Figure 2. The merits, or otherwise, of this model and the values of the parameters used are not the subject of this paper but will be discussed in a future publication in comparison with a truly microscopic model. The issue here is to determine whether a model that describes energy transfer and trapping in the reaction center may be extended to explain the antenna size dependence without a change of parameters.

Coupling the Trapping Engine to the Antenna Size Dependence. The trapping engine requires coupling to the antenna to establish if it can reproduce the trapping kinetics observed in the larger particles. To do this, we assume that energy transfer between the antenna excited states (Ant*) and the reaction center excited singlet states (RC*) is sufficiently fast, such that the antenna pigments are in quasi-static equilibrium with the reaction center singlet excited states. Thus $k_+ + k_- \gg k_{+1} + k_{-1}$ [k_+ and k_- are the forward and reverse rate constants, respectively, between Ant* and RC*; k_{+1} and k_{-1} are the forward and reverse rate constants, respectively, between RC* and RP1 (see Figures 3b and 5).] The model is then easily adapted to account for the increase in antenna size by altering the equilibrium constant between the antenna and reaction center singlet states (i.e., the ratio k_-/k_+). The effective antenna size must be used in this calculation to account for the different excited-state energies of chlorophyll *a* and chlorophyll *b* molecules. It is of note that this method of extending the model to include antenna complexes is equivalent to the scheme shown in Figure 3c, where the forward rate k_{+1} may be reduced to account for the change in the antenna size. For example, in the monomeric CP47 reaction center the increase of 10 chlorophylls may be introduced by reducing the forward rate constant k_{+1} to 0.44 of the value used in the reaction center model.

RESULTS

We present two sets of independent results, first those obtained from a comparative study of the singlet state decay kinetics on a range of samples to investigate the effect of variable antenna size on energy transfer and trapping. We also discuss a set of calculational results, which are based on an existing model that can describe the trapping dynamics in the isolated reaction center. The modeled results are not fits to the experimental data; rather they are independent of them and are based on a fixed set of parameters.

Time-correlated single photon counting has been used to give an absolute measure of the singlet state population in all samples investigated. Rather than focusing on the singlet state lifetimes, we present data that allows a comparison of the singlet state populations in each of the samples. All data were therefore scaled for the number of photons absorbed and put on an absolute scale by comparison with reaction center and dye standards, as discussed in Materials and Methods.

Table 1 shows the composition of all of the samples studied. The samples were all studied in a closed state. Thus electron transfer from the primary radical pair to Q_A could not take place. Samples may be closed by prereducing Q_A to Q_A^- with the use of either light (*50*) or chemicals (*27*). In the experiments presented here light has been used to close the samples. (In the D1/D2/cyt *b*559 isolated reaction centers and the monomeric CP47 reaction centers the quinone is lost in the isolation procedure.) To be certain that all of the samples were completely closed, power-dependent studies were performed; an example of one such study is shown in Figure 6. The fluorescence yield reaches a plateau where the sample is in a fully closed state. All experiments were carried out in this plateau region (which is antenna size dependent), ensuring that each of the samples was closed.

We show examples of the experimental data along with the multiexponential fits after deconvolution of the instrument response from three of the samples in Figure 7. This enables the comparison of data obtained from the isolated reaction center samples, dimeric CP47 RC complexes, and BBY membrane fragments.

Differences in the trapping behavior of the samples are illustrated by plotting the singlet state population at a given time. Panels a and b of Figure 8 show the singlet state population at 150 and 250 ps, respectively, and compare them to predictions using the reaction center trapping engine model shown in Figure 5. These values are obtained from fits to

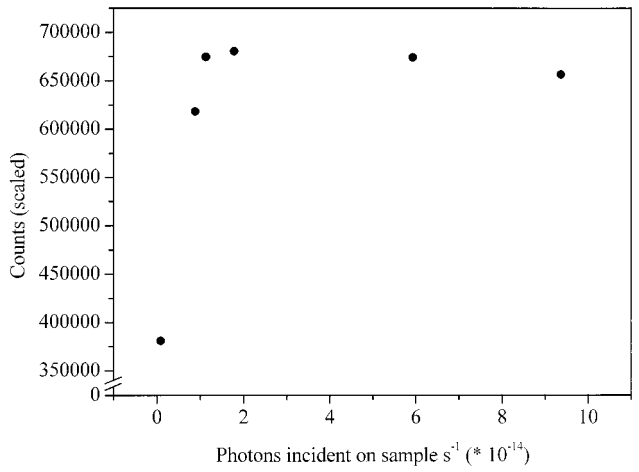

FIGURE 6: Power dependence study for BBY PS II membrane fragments. The absolute singlet state populations at 300 ps are plotted for different incident light intensities to establish when the sample is in a fully closed state.

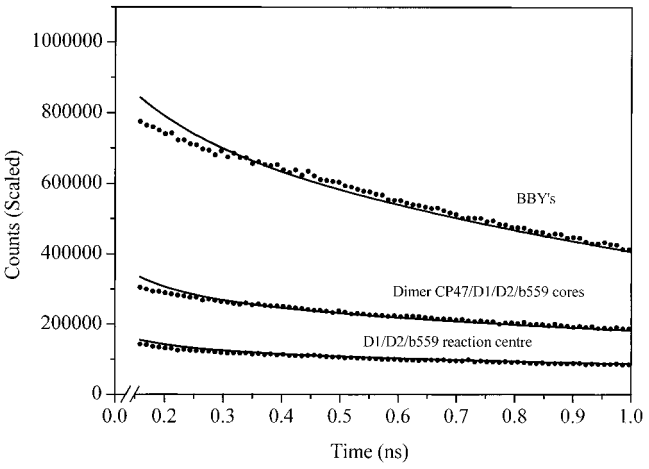

FIGURE 7: Time-resolved fluorescence data (•) and multiexponetial fits (—) from isolated D1/D2/cyt *b*559 reaction centers, dimer CP47 D1/D2/cyt *b*559 cores, and BBY PS II membrane fragments. (The fit to the reaction center data has been obtained with the combined use of transient absorption data, fluorescence up conversion, and single photon counting. The fits to the other data shown are from single photon counting data alone.)

the data and have been plotted against the relative antenna size of each sample as described in the Material and Methods. Populations at early times have not been used in order to avoid errors due to the finite length of the instrument response.

Wild-type and D1-His198Ala monomeric CP43 CP47 core complexes isolated from the cyanobacteria *Synechocystis* 6803 have also been studied. It has been established previously (*28*) that the wild-type *Synechocystis* 6803 reaction center has a shifted primary radical pair (P_{680}^+ $Pheo^-$) free energy, relative to the free energy found in reaction centers isolated from *Pisum sativum.* Mutating the D1-His198 site to D1-His198Ala in these isolated reaction center samples brought the *Synechocystis* radical pair free energy closer to that observed in reaction centers from *P. sativum.* The experiments that are presented here make the same comparison between wild-type and the D1-His198Ala mutant but in a photosystem II core preparation with antenna present. Singlet state populations at 150 and 250 ps from these samples are also shown in Figure 8.

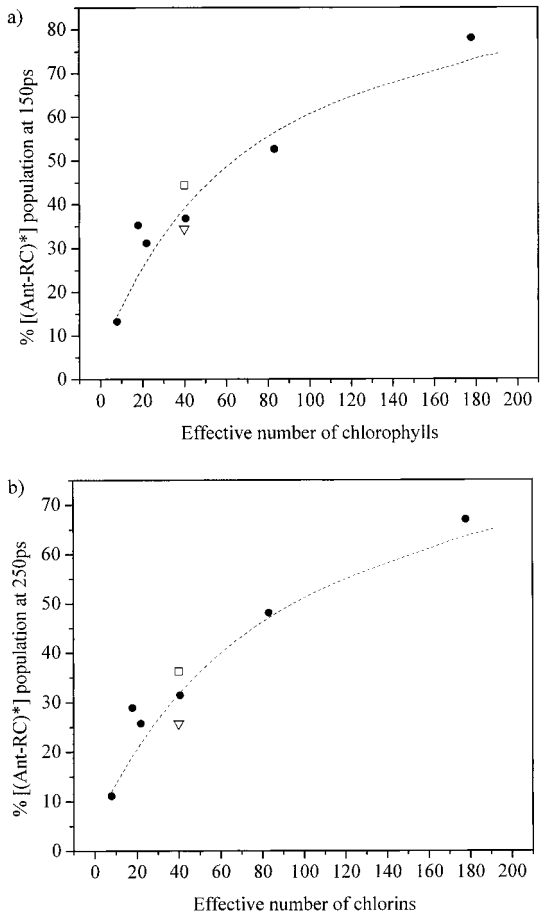

FIGURE 8: Percentage of singlet state populations at (a) 150 ps and (b) 250 ps plotted as a function of the effective chlorophyll content for each sample. Populations obtained from the fits to the data from higher plant samples (•) are compared with the model results (- - -). Data from *Synechocystis* 6803 wild type (□) and D1-His198Ala (▽) dimeric CP43 CP47 core complexes are also shown for comparison.

The remainder of this paper addresses the question of whether the time-dependent population of singlet states (i.e., energy transfer and trapping) can be predicted from our knowledge of the reaction center kinetics.

We have modeled the singlet state decay using a macroscopic model that consists of three states with inhomogeneously broadened energies of the two radical pair states (see Materials and Methods and Figure 5). This model can simulate the trapping kinetics observed experimentally from the isolated photosystem II reaction center. Without changing the parameters used in the reaction center model, we have adapted the model to establish if it could reproduce the antenna size dependence by simply accounting for the effect of the increased number of antenna molecules on the reaction center kinetics (see Materials and Methods).

By making this extension to the reaction center model, it is possible to calculate the time-dependent concentration of the singlet states in all of the particles studied here. The results of the modeling can also be compared with the experimental data by plotting the [P*] singlet state population at a time (for example, 150 or 250 ps) against the relative antenna size of each of the samples. This comparison is made in Figure 8. It is apparent that such model calculations are in excellent agreement with the experimental results.

DISCUSSION

Many previous studies have reported results from a range of different sized photosystem II particles *(27, 51−66)*. All of this previous work has focused on a kinetic analysis of the decay lifetimes from different preparations rather than investigating the absolute singlet state concentrations. It is therefore difficult to make a comparison between these studies and the data presented here. The antenna size dependence on the trapping kinetics has also been investigated in photosystem I particles by comparing the measured lifetimes with the antenna size in a number of samples (*67*).

A three-state model which allows inhomogeneously broadened energies for the two radical pair states has been used to describe the multiexponential singlet state decay kinetics observed in photosystem II reaction centers isolated from *P. sativum*. It is of note that the application of this macroscopic model does in no way discount the future use of microscopic models that allows for multiple chlorophyll anion and/or cation states, but this level of detail is not relevant to the results presented here. It may be, for example, that charge separation occurs in the reverse order to that shown here, but this will be discussed in a future publication. The key features of the reaction center trapping engine that are of importance for this work are the shallowness of the trap and the heterogeneous electron transfer kinetics.

The reaction center model was adapted to show the antenna size dependence by assuming that there is a quasi-static equilibrium between the antenna and the reaction center excited states. The antenna size was then simply included by accounting for the effect of the increased number of accessible singlet states on the electron transfer kinetics, via a change in the quasi-static equilibrium constant.

Some previous work (*68*, *69*) has raised concerns regarding how far the photochemical properties of the remaining pigments in isolated D1/D2/cyt *b*559 complexes have been altered in comparison to intact photosystem II. We show here, however, that the trapping action of the primary radical pair formation in isolated photosystem II reaction centers is indeed identical to that of the reaction centers within larger photosystem II particles, even up to membrane fragments (BBY's).

It has been suggested that energy transfer from the antenna to the reaction center may be rate limiting (*70*, *71*). Our results, however, suggest that energy transfer is not the rate-limiting step in the trapping process. As there is no energy transfer bottleneck in the isolated reaction center (*10*, *11*, *16*), the consistency with larger particles indicates that there is no bottleneck in these samples either.

There appears to be no major discrepancy between those particles that lack Q_A and those in which Q_A was prereduced by light. It would be surprising, though not impossible, for the presence of Q_A^- to leave the trapping kinetics unaffected. These observations therefore contribute some minor evidence that either Q_A^- becomes protonated under the conditions used here or that the presence of Q_A^- does not affect primary charge separation.

Both the experimental and the modeled results shown in panels a and b of Figure 8 show a distinct curvature in the relationship between the singlet state population and particle size. The reason for this is most clearly illustrated for the simple case of a two-state model. Consider the process:

$$(\text{Ant RC})^* \underset{k_{-1}}{\overset{k_{+1}}{\Longleftrightarrow}} \text{RP}_1$$

Mathematically the effect of antenna size can be modeled by simply altering the forward rate of electron transfer k_{+1} if a quasi-static equilibrium between the antenna (Ant*) and the reaction center singlet states (RC*) is assumed (as explained in Materials and Methods and Figure 3). Assuming that there is no nonradiative decay of the singlet states, the singlet state concentration at equilibrium [(Ant RC)*] may be calculated to be

$$[(\text{Ant RC})^*] = \frac{1}{(k_{+1}/k_{-1}) + 1} \qquad (2)$$

Thus as k_{+1} decreases due to the increase in particle size, the $+1$ term becomes dominant, which results in the curvature observed in both the modeled and experimental data shown in Figure 8.

We have also studied core samples that have had their radical pair free energies modulated using site-directed mutagenesis. This has enabled us to establish that changing the radical pair free energy does indeed have an effect in larger particles. It is known that wild-type reaction centers from *Synechocystis* PCC 6830 have raised radical pair free energies with respect to those found in *P. sativum* (*28*). It was also found that, when the wild-type reaction center was mutated to His198Ala, the radical pair free energy was lowered, such that its energy was closer to that found in *P. sativum* reaction centers. Figure 8 shows that a similar effect has been observed in the *Synechocystis* core data. The singlet state populations at 150 and 250 ps from the *Synechocystis* His198Ala mutant are compared with the *Synechocystis* wild-type and higher plant data. These results would suggest that the equilibrium between the excited singlet states and the primary radical pair states is shifted toward the radical pair in the His198Ala mutant. This implies that the free energy of the radical pair is lowered with respect to the wild type as observed in the equivalent reaction center mutant experiments.

It is not immediately obvious why a shallow radical pair/singlet state equilibrium and slow charge separation should be found in photosystem II when they are not observed in, for example, purple bacteria. A shallow equilibrium between the antenna and reaction center in photosystem II will facilitate regulation via nonphotochemical quenching. One possible interpretation of these findings is that photosystem II is optimized for regulation rather than for efficiency.

CONCLUSIONS

(1) An inhomogeneous three-state model can adequately describe the trapping dynamics in the isolated photosystem II reaction center and reaction center mutants.

(2) This representation of the photosystem II reaction center successfully describes the antenna size dependence of the trapping in a range of photosystem II particles.

(3) Slow trapping of excitation energy via the formation of a shallow primary radical pair state P_{680}^+ $Pheo^-$ seems to be a genuine feature of the bioenergetics of photosystem II.

ACKNOWLEDGMENT

We thank Chris Barnett for excellent technical assistance.

REFERENCES

1. Diner, B. A., and Babcock, G. T. (1996) in *Oxygenic Photosynthesis: The Light Reactions* (Ort, D. R., and Yocum, C. F., Eds.) pp 213−247, Kluwer Academic Publishers, Boston, MA.
2. Zheleva, D., Hankamer, B., and Barber, J. (1996) *Biochemistry 35*, 15074−15079.
3. Eijckelhoff, C., and Dekker, J. P. (1995) *Biochim. Biophys. Acta 1231*, 21−28.
4. Durrant, J. R., Klug, D. R., Kwa, S. L. S., vanGrondelle, R., and Porter, G. (1995) *Proc. Natl. Acad. Sci. U.S.A. 92*, 4788−4802.
5. Danielus, R. V., Satoh, K., vanKan, P. J. M., Plijter, J. J., Nuijs, A. M., and vanGorkom, H. J. (1987) *FEBS Lett. 213*, 241−244.
6. Durrant, J. R., Hastings, G., Joseph, D. M., Barber, J., Porter, G., and Klug, D. R. (1992) *Proc. Natl. Acad. Sci. U.S.A. 89*, 11632−11636.
7. Durrant, J. R., Hastings, G., Joseph, D. M., Barber, J., Porter, G., and Klug, D. R. (1993) *Biochemistry 32*, 8259−8267.
8. Hastings, G., Durrant, J. R., Barber, J., Porter, G., and Klug, D. R. (1992) *Biochemistry 31*, 7638−7647.
9. Klug, D. R., Rech, T., Joseph, D. M., Barber, J., Durrant, J. R., and Porter, G. (1995) *Chem. Phys. 194*, 433−442.
10. Rech, T., Durrant, J. R., Joseph, D. M., Barber, J., Porter, G., and Klug, D. R. (1994) *Biochemistry 33*, 14678−14774.
11. Merry, S. A. P., Kumazaki, S., Tachibana, Y., Joseph, D. M., Porter, G., Yoshihara, K., Durrant, J. R., and Klug, D. R. (1996) *J. Phys. Chem. 100*, 10469−10478.
12. Barber, J., and Andersson, B. (1992) *Trends Biochem. Sci. 17*, 61−66.
13. Horton, P., Ruban, A. V., and Walters, R. G. (1996) *Annu. Rev. Plant Physiol. Plant Mol. Biol. 47*, 655−684.
14. Nanba, O., and Satoh, K. (1987) *Proc. Natl. Acad. Sci. U.S.A. 84*, 109−112.
15. Barber, J., Chapman, D. J., and Telfer, A. (1987) *FEBS Lett. 220*, 67−73.
16. Vacha, F., Joseph, D. M., Durrant, J. R., Telfer, A., Klug, D. R., Porter, G., and Barber, J. (1995) *Proc. Natl. Acad. Sci. U.S.A. 92*, 2929−2933.
17. Kumazaki, S., Joseph, D. M., Crystall, B., Tachibana, Y., Durrant, J. R., Barber, J., Porter, G., Yoshihara, K., and Klug, D. R. (1995) in *Photosynthesis: From light to Biosphere* (Mathis, P., Ed.) pp 883−886, Kluwer Academic Publishers, The Netherlands.
18. Greenfield, S. R., Seibert, M., Govindjee, and Wasielewski, M. R. (1997) *J. Phys. Chem. B 101*, 2251−2255.
19. Donovan, B., Walker, L. A., II, Yocum, C. F., and Sension, R. J. (1996) *J. Phys. Chem. 100*, 1945−1949.
20. Muller, M. G., Hucke, M., Reus, M., and Holzwarth, A. R. (1996) *J. Phys. Chem. 100*, 9527−9536.
21. Groot, M. L., vanMourik, F., Eijckelhoff, C., vanStokkum, I. H. M., Dekker, J. P., and vanGrondelle, R. (1997) *Proc. Natl. Acad. Sci. U.S.A. 94*, 4389−4394.
22. Booth, P. J., Crystall, B., Giorgi, L. B., Barber, J., Klug, D. R., and Porter, G. (1990) *Biochim. Biophys. Acta 1016*, 141−152.
23. Volk, M., Gilbert, M., Rousseau, G., Richter, M., Ogrodnik, A., and Michel-Beyerle, M.-E. (1993) *FEBS Lett. 336*, 357−362.
24. Goldstein, R. A., Takiff, L., and Boxer, S. G. (1988) *Biochim. Biophys. Acta 934*, 253−263.
25. Ogrodnik, A., Volk, M., Letterer, R., Feick, R., and Michel-Beyerle, M. E. (1988) *Biochim. Biophys. Acta 936*, 361−371.
26. Hörber, J. K. H., Göbel, W., Ogrodnik, A., Michel-Beyerle, M. E., and Cogdell, R. J. (1986) *FEBS Lett. 198*, 273−278.
27. Schatz, G. H., Brock, H., and Holzwarth, A. R. (1987) *Proc. Natl. Acad. Sci. U.S.A. 84*, 8414−8418.
28. Merry, S. A. P., Nixon, P. J., Barter, L. M. C., Schilstra, M., Porter, G., Barber, J., Durrant, J. R., and Klug, D. R. (1998) *Biochemistry 37*, 17439−17447.
29. Leegwater, J. A., Durrant, J. R., and Klug, D. R. (1997) *J. Phys. Chem. B 101*, 7205−7210.
30. Peterman, E. J. G., vanAmerongen, H., vanGrondelle, R., and Dekker, J. P. (1998) *Proc. Natl. Acad. Sci. U.S.A. 95*, 6128−6133.
31. Kwa, S. L. S., Eijckelhoff, C., vanGrondelle, R., and Dekker, J. P. (1994) *J. Phys. Chem. 98*, 7702−7711.
32. Chapman, D. J., Gounaris, K., and Barber, J. (1991) in *Methods in Plant Biochemistry* (Rogers, L., Ed.) pp 171−193, Academic Press Ltd., London.
33. Boekema, D. J., Hankamer, B., Bald, D., Kruip, J., Nield, J., Boonstra, A. F., Barber, J., and Rogner, M. (1995) *Proc. Natl. Acad. Sci. U.S.A. 92*, 175−179.
34. Zheleva, D., Sharma, J., Panico, M., Morris, H. R., and Barber, J. (1998) *J. Biol. Chem. 273*, 16122−16127.
35. Bianchetti, M., Zheleva, D., Deak, Z., Zharmuhamedov, S., Klimov, V., Nugent, J., Vass, I., and Barber, J. (1998) *J. Biol. Chem. 273*, 16128−16133.
36. Hankamer, B., Nield, J., Zhelva, D., Boekema, E., Jansson, S., and Barber, J. (1997) *Eur. J. Biochem. 243*, 422−429.
37. Boekema, E. J., Nield, J., Hankamer, B., and Barber, J. (1998) *Eur. J. Biochem. 252*, 268−276.
38. Berthold, D. A., Babcock, G. T., and Yocum, C. F. (1981) *FEBS Lett. 134*, 231−234.
39. Schilstra, M. J., Rappaport, F., Nugent, J. H. A., Barnett, C. J., and Klug, D. R. (1998) *Biochemistry 37*, 3974−3981.
40. Tang, X.-S., Zheng, M., Chisholm, D. A., Dismukes, G. C., and Diner, B. A. (1996) *Biochemistry 35*, 1475−1484.
41. Booth, P. J., Crystall, B., Ahmad, I., Barber, J., Porter, G., and Klug, D. R. (1991) *Biochemistry 30*, 7573−7586.
42. vanGrondelle, R. (1985) *Biochim. Biophys. Acta 811*, 147−195.
43. Schatz, G. H., Brock, H., and Holzwarth, A. R. (1988) *Biophys. J. 54*, 397−405.
44. Durrant, J. R., Nixon, P. J., Barber, J., and Klug, D. R. (1998) (Garab, G., Ed.) pp 1041−1044, Kluwer Academic Publishers, The Netherlands.
45. Ogrodnik, A., Keupp, W., Volk, M., Aumeier, G., and Michelbeyerle, M. E. (1994) *J. Phys. Chem. 98*, 3432−3439.
46. Wang, Z., Pearlstein, R. M., Jia, Y., Fleming, G. R., and Norris, J. R. (1993) *Chem. Phys. 176*, 421−425.
47. Groot, M.-L., Petermann, E. J. G., vanKan, P. J. M., vanStokkum, I. H. M., Dekker, J. P., and Grondelle, R. v. (1994) *Biophys. J. 67*, 318−330.
48. Durrant, J. R., Porter, G., Barber, J., and Klug, D. R. (1995) in *10th International Photosynthesis Congress* (Mathis, P., Ed.) pp 611−614, Kluwer Academic Publishers, The Netherlands.
49. Marcus, R. A., and Sutin, N. (1985) *Biochim. Biophys. Acta 811*, 265−322.
50. Schelvis, J. P. M., Germano, M., Aartsma, T. J., and vanGorkom, H. J. (1995) *Biochim. Biophys. Acta 1230*, 165−169.
51. Berens, S. J., Scheele, J., Butler, W. L., and Madge, D. (1985) *Photochem. Photobiol. 42*, 51−57.
52. Green, B. R., Karukstis, K. K., and Sauer, K. (1984) *Biochim. Biophys. Acta 767*, 574−581.
53. Gulotty, R. J., Fleming, G. R., and Alberte, R. S. (1982) *Biochim. Biophys. Acta 682*, 322−331.
54. Gulotty, R. J., Mets, L., Alberte, R. S., and Fleming, G. R. (1985) *Photochem. Photobiol. 41*, 487−496.
55. Haehnel, W., Nairn, J. A., Reisberg, P., and Sauer, K. (1982) *Biochim. Biophys. Acta 680*, 161−173.
56. Haehnel, W., Holzwarth, A. R., and Wendler, J. (1983) *Photochem. Photobiol. 37*, 435−443.
57. Hodges, M., and Moya, I. (1986) *Biochim. Biophys. Acta 849*, 193−202.
58. Holzwarth, A. R., Wendler, J., and Haehnel, W. (1985) *Biochim. Biophys. Acta 807*, 155−167.

59. Hodges, M., and Moya, I. (1987) *Biochim. Biophys. Acta 892*, 42−47.
60. Kraukstis, K. K., and Sauer, K. (1984) *Biochim. Biophys. Acta 766*, 148−155.
61. Keuper, H. J. K., and Sauer, K. (1989) *Photosynth. Res. 20*, 85−103.
62. Moya, I., Hodges, M., and Barbet, J.-C. (1986) *FEBS Lett. 198*, 256−262.
63. Moya, I., Hodges, M., Briantais, J.-M., and Hervo, G. (1986) *Photosynth. Res. 10*, 319−325.
64. Nairn, J. A., Haehnel, W., Reisberg, P., and Sauer, K. (1982) *Biochim. Biophys. Acta 682*, 420−429.
65. vanMieghem, F. J. E., Searle, G. F. W., Rutherford, A. W., and Schaafsma, T. J. (1992) *Biochim. Biophys. Acta 1100*, 198−206.
66. Freiberg, A., Timpmann, K., Moskalenko, A. A., and Kuznetsova, N. Y. (1993) *Biochim. Biophys. Acta 1184*, 45−53.
67. Owens, T. G., Webb, S. P., Mets, L., Alberte, R. S., and Fleming, G. R. (1987) *Proc. Natl. Acad. Sci. U.S.A. 84*, 1532−1536.
68. Hillmann, B., Brettel, K., vanMieghem, F., Kamlowski, A., Rutherford, A. W., and Schlodder, E. (1995) *Biochemistry 34*, 4814−4827.
69. Renger, G. (1992) in *The Photosystems: Structure, Function and Molecular Biology* (Barber, J., Ed.) pp 45−99, Elsevier Science Publishers, New York.
70. vanGrondelle, R., Dekker, J. P., Gillbro, T., and Sundstrom, V. (1994) *Biochim. Biophys. Acta 1187*, 1−65.
71. Visser, H. M., Kleima, F. J., vanStokkum, I. H. M., vanGrondelle, R., and vanAmerongen, H. (1996) *Chem. Phys. 210*, 297−312.

BI001724Q